

The Angular Momentum Problem in Cosmological Simulations of Disk Galaxy Formation

Franziska Piontek and Matthias Steinmetz
Astrophysikalisches Institut Potsdam, An der Sternwarte 16, 14482 Potsdam, Germany

ABSTRACT

We conduct a systematic study of the angular momentum problem in numerical simulations of disk galaxy formation. We investigate the role of numerical resolution using a semi-cosmological setup which combines an efficient use of the number of particles in an isolated halo while preserving the hierarchical build-up of the disk through the merging of clumps. We perform the same simulation varying the resolution over 4 orders of magnitude. Independent on the level of resolution, the loss of angular momentum stays the same and can be tied to dynamical friction during the build-up phase. This is confirmed in a cosmological simulation. We also perform simulations including star formation and star formation and supernova feedback. While the former has no influence on the angular momentum problem, the latter reduces the loss to a level potentially in agreement with observations. This is achieved through a suppression of early star formation and therefore the formation of a large, slowly rotating bulge. We conclude that feedback is a critical component to achieve realistic disk galaxies in cosmological simulations. Numerical resolution is important, but by itself not capable of solving the angular momentum problem.

Key words: galaxies: spiral - formation - evolution - methods: N -body simulations - hydrodynamics

1 INTRODUCTION

The prevailing picture of galaxy formation was formulated almost 30 years ago by White & Rees (1978) and Fall & Efstathiou (1980). Gas falls into the potential wells of hierarchically growing dark matter structures and is additionally governed by dissipational processes. The idea of dark matter halos acquiring angular momentum through tidal torques from surrounding large scale structure was first developed by Strömberg (1934) and Hoyle (1949) and later quantified by Peebles (1969), Doroshkevich (1970) and White (1984). It results in slowly rotating dark matter halos (Barnes & Efstathiou 1987; Steinmetz & Bartelmann 1995). The gas within the halo acquires the same specific angular momentum, but it can cool, therefore collapses and, under of conservation of angular momentum, forms disks (Mo, Mao & White 1998). Stars are formed due to the fragmentation of the gas disks, and spheroids are formed during the interaction and merging of disks (Toomre & Toomre 1972). The detailed interaction of gas, stars and related physical processes make this a very complex problem, which needs to be addressed through numerical simulations. This is a twofold challenge. The first challenge is posed by the large dynamic range of scales which are encountered, from the tens of Mpc scales of halo and galaxy interaction during assembly to the sub-pc scales of star formation. The second

challenge stems from physical processes like star formation and feedback, which happen on scales below the resolution of most present day cosmological simulations. It is thus not so surprising that, despite many efforts in the past years, disk galaxies with realistic properties remain elusive in simulated universes. Especially bulge-less disks, which have been shown to exist in non-negligible numbers (Kautsch et al. 2006) in the nearby universe, have not been produced in a simulation up to this point.

One of the major problems encountered in numerical simulations of disk formation is the so called angular momentum catastrophe (Navarro & Benz 1991). Early simulations all resulted in small, highly centrally concentrated disks with dominating bulges (for example Navarro & White 1994; Steinmetz & Navarro 1999; Navarro & Steinmetz 2000) after loosing large amounts of angular momentum during the formation. As four main causes have been proposed: (1) lack of resolution (Governato et al. 2004; Kaufmann et al. 2007); (2) an artificial transfer of angular momentum from the cold disk at the interface to the hot halo (Okamoto et al. 2005); (3) disk instabilities leading to fragmentation (Robertson et al. 2004); (4) merging of substructure leading to transfer of angular momentum to the outer halo via dynamical friction (Navarro & Benz 1991; Navarro & White 1994). The second and third effect can be avoided with an improved imple-

mentation of gas physics (a decoupling of hot and cold gas phases for the second effect as suggested by Okamoto et al. (2005) or a multiphase medium for the third effect according to Robertson et al. (2004)). Low numerical resolution, the first effect, can cause artificial loss of angular momentum through a variety of effects like numerical two-body heating due to the large mass difference between dark matter and gas particles (Steinmetz & White 1997; Mayer 2005), artificial viscosity, an incorrect pressure estimate in the standard SPH method for particles with significant temperature differences (as happens for example at the edge of the disk), and an artificial asymmetry of the disk causing gravitational torques from the surrounding halo. These problems can be remedied with larger numbers of particles in the disk. Others, like a correct modeling of the disk center where velocity gradients are steep and angular momentum is easily lost, or the formation of bars, which can transport angular momentum outward efficiently, are difficult to address even with very large particle numbers. While these effects have been demonstrated to operate in well established disks and smooth collapse scenarios (Kaufmann et al. 2007), it still needs to be demonstrated to what extent they are responsible for the angular momentum loss seen in fully cosmological large scale structure simulations.

As opposed to the first three effects, the fourth, merging of substructure, is a physical effect which is natural to Λ CDM. It affects dark matter as well as gas, and angular momentum is lost through dynamical friction of interacting and merging clumps. The most efficient mechanism to prevent angular momentum loss through this process is to prevent the formation of too many clumps. For this, two scenarios have been discussed. The first one involves a change in the cosmological model from cold to warm dark matter (WDM). While leaving the large scales untouched, this results in a smoothing of small scales of the power spectrum, and therefore less substructure and a smoother accretion of baryons onto dark matter halos instead of dense clumps susceptible to dynamical friction. Sommer-Larsen & Dolgov (2001) successfully showed that this leads to an alleviation of the angular momentum problem, which puts doubt on the claim that the angular momentum problem is mainly a resolution issue. It can also help to solve what is known as the "missing satellite problem" in Λ CDM, a large excess in dark matter substructure predicted by numerical simulations compared to observed numbers of satellite galaxies (Götz & Sommer-Larsen 2003). However, observational constraints on the mass of dark matter particles, for example by the redshift of re-ionization (which is delayed significantly in a WDM universe due to the lack of low mass halos), already allow only varieties which are tepid at most (Viel et al. 2008). In the second scenario preventing the gas from forming small, dense clumps before entering the main halo, the thermal energy of the gas is increased via physical processes like feedback from supernova explosions or stellar winds. We will address this in the second part of this paper.

In this paper, we will focus on the role of resolution and feedback with respect to the angular momentum problem in numerical simulations of disk galaxy formation. We present a detailed, systematic study of resolution effects in isolated but semi-cosmological halos preserving the essence of the hierarchical formation history, and also test the results in fully cosmological runs. The study also covers the effects of

various physical processes ranging from simulations including only radiative cooling over the inclusion of simple star formation to the application of a model for supernova feedback. The paper is organized as follows: in §2 we describe the code and the initial conditions we use. In §3 we present the results on the angular momentum problem in simulations including only gravity and radiative cooling. §4 discusses the impact of star formation and the feedback model and in §5 we summarize and discuss our results.

2 CODE AND INITIAL CONDITIONS

All simulations are based on the WMAP3 cosmology (Spergel et al. 2007) with $H_0=73 \text{ km s}^{-1}\text{Mpc}^{-1}$, $\sigma_8 = 0.75$, $n_s = 0.9$, $\Omega_0 = 0.24$, $\Omega_\Lambda = 0.76$ and $\Omega_b = 0.04$. We use the N-body code GADGET2 (Springel 2005) in a version including radiative cooling based on Katz et al. (1996). To minimize the number of free parameters we do not include a UV background. The gas is treated within the Smoothed Particle Hydrodynamics (SPH) framework (Gingold & Monaghan (1977), Lucy (1977)). In the following, we explain our implementation of star formation and supernova feedback.

2.1 Star formation and feedback

Our basic star formation model follows Katz (1992) and Navarro & White (1994). The main criteria for either spawning a new star particle from a gas particle or turning the gas particle into a star particle (depending on the gas mass) are:

- (1) $\rho > \rho_{\text{crit}}$, where we choose¹ $\rho_{\text{crit}}=7 \times 10^{-26} \text{ g cm}^{-3}$
- (2) $\nabla \cdot \vec{v} < 0$
- (3) $T < 3 \times 10^4 \text{ K}$.

The star formation rate is guided by a basic Schmidt law (Schmidt 1959), but expressed in physical density as

$$\frac{d\rho_\star}{dt} = c_\star \frac{\rho_{\text{gas}}}{t_\star} \quad (1)$$

where c_\star is a dimensionless parameter regulating the star formation efficiency (we use $c_\star=0.1$, in agreement with observations by Duerr et al. (1982) for the ISM in the Milky Way) and

$$t_\star = \max(t_{\text{dyn}}, t_{\text{cool}}), \quad t_{\text{dyn}} = (4\pi G\rho)^{-1/2}. \quad (2)$$

We use a stochastic approach to star formation, so the probability to form a star particle during a given timestep Δt is given by

$$p = \frac{m_{\text{gas}}}{m_{\text{gas,orig}}\epsilon} (1 - e^{-c_\star \frac{\Delta t}{t_\star}}). \quad (3)$$

ϵ is a parameter giving the fraction of the gas mass turned into a star or, alternatively interpreted, the number of generations of stars. We generally use $\epsilon=2$ to prevent too much increase in the number of particles.

¹ This choice of density corresponds to a region where the cooling time is always shorter than the dynamical time, resulting in rapid cooling to the cut-off temperature of the cooling curve (10^4K) where the Jeans instability criterion (sound crossing time is larger than the dynamical time) is almost always fulfilled (Navarro & White 1994).

We include the most basic but also probably most influential type of stellar feedback: energy output from the late stages of the evolution of massive stars ($M > 8 M_{\odot}$). This is usually referred to as supernova feedback, but actually covers all types of energetic feedback which are not resolved in this study. The model implemented here showed the best performance in a more extensive study of feedback models which is presented in Piontek & Steinmetz (2009b). As in all N-body simulations, each “star particle” represents a whole population of stars of total mass M_{\star} (which depends on resolution). For this we assume a Miller-Scalo initial mass function (IMF) (IMF, Miller & Scalo 1979) with a lower cutoff of $0.1 M_{\odot}$ and an upper cutoff of $100 M_{\odot}$:

$$\xi(M) = M_{\star} A \begin{cases} M^{-1.25} & 0.1 < M < 1 M_{\odot} \\ M^{-2} & 1 < M < 2 M_{\odot} \\ 2^{0.3} M^{-2.3} & 2 < M < 10 M_{\odot} \\ 10 2^{0.3} M^{-3.3} & 10 < M < 100 M_{\odot} \end{cases} \quad (4)$$

where $A = 0.284350751$ and M_{\star} is the mass of the stellar population, in our case of the star particle. Stars with masses between 8 and $100 M_{\odot}$ explode as type II supernova and each explosion is assumed to yield an energy of 10^{51} ergs. This corresponds to an energy of 1.21×10^{49} erg per solar mass formed. To avoid numerical artefacts related to abrupt changes in the thermal properties of the gas which cannot be resolved, the energy is returned to the surrounding gas over time following an exponential approach using

$$\Delta E(t) = E_{SN} \frac{t - t_{\star}}{t_{SN}} e^{-\frac{t - t_{\star}}{t_{SN}}} \frac{\Delta t}{t_{SN}}. \quad (5)$$

Here, E_{SN} is the total supernova energy, t_{\star} is the time when the star particle was created and t_{SN} is a typical time scale (we use 20 Myr as the lifetime of a $8 M_{\odot}$ star). This energy is smoothed over the neighboring gas particles using the SPH smoothing kernel, so each neighbor gets an energy of

$$\Delta E_{SN,i} = \Delta E(t) \frac{W(|\vec{r}_i - \vec{r}_{\star}|, h_{\star}) M_i}{\rho_{\star}}. \quad (6)$$

h_{\star} is the smoothing length and the most important parameter here. This is a variable length scale calculated similar to the gas smoothing length in GADGET2 (the mass within the smoothing sphere is kept constant).

Katz (1992) and Steinmetz & Müller (1995) found that supernova feedback energy is radiated away very quickly in the simulations, since star formation by definition occurs in dense regions with short cooling times. Consequently, in these early simulations, feedback had little impact. In more realistic ISM models this does not happen due to the multiphase nature of the gas, but it is computationally demanding, if at all possible, to achieve enough resolution to directly simulate this. One method to prevent this immediate re-radiation was suggested by Gerritsen (1997) and later Thacker & Couchman (2000). It involves turning off radiative cooling in gas particles receiving feedback energy and evolving them adiabatically for a given time. We adopt this method and turn off the cooling locally for a time of 20 Myr (in agreement with earlier simulations and similar to the lifetime of a supernova shell).

2.2 Isolated initial conditions

It is our goal to isolate the root cause of and find a solution for the angular momentum problem. In a fully cosmological

simulation, this is difficult, since the resolution for a given halo and particularly for the forming galaxy is limited and the hierarchical merging processes are likely to destroy disk progenitors. Therefore we first perform a controlled experiment for an isolated halo, and then verify our conclusions in a cosmological box. However, a completely isolated and idealized setup consisting of an NFW halo² in combination with a hot gas halo, as in Kaufmann et al. (2007), is too artificial to probe the relevant physics, since it completely lacks any merging in the formation process. To be more realistic with the same benefits of high resolution in the gas disk and no major mergers destroying it, we use a semi-cosmological setup as in Katz (1991). We start with a cosmological box with a side length of $2 \text{ h}^{-1} \text{ Mpc}$, large enough to host one Milky Way-type halo, but lacking all large scale structure. Centering the forming halo, we cut out a sphere with $1 \text{ h}^{-1} \text{ Mpc}$ radius which is simulated in physical coordinates and with vacuum boundary conditions. To mimic the missing large scale effects, we apply an overdensity of 3σ and put the sphere into solid body rotation with a spin parameter of $\lambda = 0.08$. This is higher than what is typical for dark matter halos ($\lambda \approx 0.04$ Bullock et al. 2001), but will ensure the formation of a large rotationally supported and stable gas disk. We include gas particles by splitting each dark matter particle into a gas and a dark matter particle with the mass ratio given by the density parameters. The initial redshift of the simulations is $z=75$. For our resolution study, we create the same initial conditions with four different resolutions, based on boxes with 16^3 , 32^3 , 64^3 and 128^3 dark matter particles. This corresponds to spheres with 2×10^3 , 2×10^4 , 1.4×10^5 and 1.1×10^6 particles each in gas and dark matter. We use a gravitational softening growing proportional to the scale factor for $z > 10$ and staying fixed in physical coordinates after $z=10$, at a value of $1 \text{ h}^{-1} \text{ kpc}$ for the 3 lower resolutions and $0.25 \text{ h}^{-1} \text{ kpc}$ for the highest resolution, for both gas and dark matter particles. We also tested higher softenings for the two lowest resolutions - 4 kpc h^{-1} for 16^3 and 2 kpc h^{-1} for 32^3 , which is in better agreement with the criterion derived by Power et al. (2003). However, the results for these runs do not differ significantly from those with smaller softening length, so they are not presented here.

2.3 Cosmological initial conditions

From a cosmological $64^3 \text{ h}^{-1} \text{ Mpc}$ box we resimulate a halo promising to host a Milky Way-type galaxy. The crucial selection features are the halo mass ($M_{\text{halo}} \simeq 10^{12} \text{ h}^{-1} M_{\odot}$), a relatively quiet merging history (the redshift of the last major merger with mass ratios of 1:3 and 1:10 are $z=3.63$ and $z=2$ respectively), a high spin parameter ($\lambda = 0.057$) and no halo with equal or larger mass within a distance of 2 Mpc . We perform runs with three levels of resolution in the resimulated region corresponding to an effective resolution of 512^3 , 1024^3 and 2048^3 . This corresponds to particle masses for dark matter (gas) of $1.47 \times 10^8 M_{\odot}$ ($3.1 \times 10^7 M_{\odot}$), $1.86 \times 10^7 M_{\odot}$ ($3.71 \times 10^6 M_{\odot}$) and $2.32 \times 10^6 M_{\odot}$ ($4.64 \times 10^5 M_{\odot}$) respectively. Star particles have half the mass of the initial

² A halo with the density profile as in equation 10, quantified by Navarro, Frenk & White (1997).

gas particle mass. A gravitational softening of 4 (3), 2 (1.5) and 1 (0.75) h^{-1} kpc is used.

2.4 Analysis of a simulated galaxy

We define our halos using the virial radius R_{vir} , which is the radius where $\rho(r) = \Delta\rho_c$ with $\rho_c = 3H_0^2/(8\pi G)$ and $\Delta = 18\pi^2 + 82x - 39x^2$, $x = \Omega_0(1+z)^3/(\Omega_0(1+z)^3 + \Omega_\Lambda) - 1$. The cold gas ($T < 3 \times 10^4$ K) in the center of the halo makes up a clearly defined disk. In runs without star formation and feedback, all cold gas ends up in that disk. In the runs with feedback, some hot gas surrounding the cold gas is present, but the disk can still be distinguished clearly. When star formation is included, stars within the disk radius are defined as being part of the galaxy. Since the rotationally supported gas disk gives a clear axis of symmetry, we rotate the system to have this axis aligned with the axis in z direction and the disk in the x - y plane. The total specific angular momentum j of the disk is then computed by summing over all disk particles, with respect to the center of mass of these particles. It is given by

$$j = \frac{|\vec{J}|}{\sum m_i} \quad (7)$$

where

$$\vec{J} = \sum m_i(\vec{r}_i - \vec{R}_{\text{COM}}) \times (\vec{v}_i - \vec{v}_{\text{COM}}). \quad (8)$$

To compute the time evolution of the angular momentum, all particles belonging to the galaxy at $z=0$ are tracked back in time and the angular momentum is calculated in earlier snapshots for these particles with respect to the center of mass at the time. When star formation is included, the progenitor gas particles are used at the time when stars have not formed yet.

3 THE ANGULAR MOMENTUM PROBLEM IN SIMULATIONS WITH RADIATIVE COOLING

Our first, most basic set of runs includes dark matter and gas and the latter is subject to radiative cooling only. Star formation and feedback are turned off. This should enable us to pinpoint the processes responsible for the loss of angular momentum and investigate the role resolution can play to avoid this process without the additional, probably positive effects feedback should have.

3.1 Isolated initial conditions

We first analyze the results of our controlled semi-cosmological, isolated experiment in four different resolutions. Some characteristic parameters of the different runs are summarized in Table 1.

3.1.1 The resulting disk

The evolution in the semi-cosmological setup is illustrated in Figure 1 for the 32^3 resolution. Since it is a physical coordinate system, initially the sphere expands following the expansion of the universe. The redshifts of turnaround at

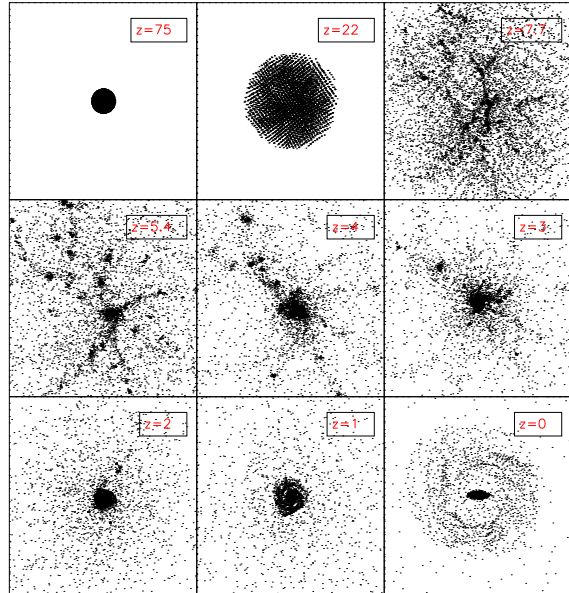


Figure 1. The formation of the disk in our 32^3 sphere from the starting redshift of 75 until $z=0$. Each plot has a side length of 280 physical kpc except the last one which zooms in to 80 kpc side length.

$z \sim 12$ and collapse at $z \sim 8$ agree well with analytical expectations based on Lokas & Hoffman (2001). Small, cold gas clumps merge to form a central disk. This process is finished around $z=1$ after which there is no longer any significant evolution. There is no late infall owing to the missing large scale environment. The disk can be described as a central overdense clump with a radius of about 5 kpc containing up to 80% of the total disk mass, and a thin outer disk. The resulting disk is unchanged with increasing resolution.

We examine the stability of the disk with respect to the Toomre Q parameter (Toomre 1964)

$$Q(r) = \frac{c_s \kappa}{\pi G \Sigma_g} \quad (9)$$

where c_s is the effective soundspeed, κ the epicyclic frequency and Σ_g the gas surface density. The disk is stable where $Q(r) > 1.0$. As illustrated in Figure 2, in our case the disk is clearly unstable in the innermost, compact region, and only marginally stable in the outer parts (solid curve). Star formation can therefore happen in the disk. It could be stabilized if the gas were to remain hot with a minimum temperature of 5×10^4 K, as shown by the dashed line in Figure 2.

3.1.2 Verification of the setup with an analytical model

We attempt a verification of our semi-cosmological initial conditions setup by comparing the resulting disk to predictions obtained with the analytical galaxy formation model by Mo, Mao & White (1998) (hereafter MMW). In their model MMW derive the properties of disks (like mass, scale radius, central surface density) from the density profile of the dark matter halo and its angular momentum under the

	16 ³	32 ³	64 ³	128 ³	cosmological run
DM particle mass [M_\odot]	3.62×10^8	4.5×10^7	5.64×10^6	7.05×10^5	1.86×10^7
gas particle mass [M_\odot]	7.24×10^7	9.01×10^6	1.13×10^6	1.41×10^5	3.71×10^6
# of gas particles in disk	1510	12710	106319	606895 ($z=1.7$)	38856
ϵ [h^{-1} kpc]	1	1	1	0.25	1.5
R_{vir} [kpc]	248	251	251		292
V_{vir} [km s^{-1}]	123.38	124.45	124.55		145.45
M_{vir} [M_\odot]	8.73×10^{11}	8.99×10^{11}	9.01×10^{11}		1.21×10^{12}
c	28.04	29.68	30.542		10.13
λ	0.083	0.088	0.083		0.055

Table 1. Characteristic parameters for the semi-cosmological simulations with increasing resolution and for the cosmological run with an effective resolution of 1024^3 particles in the high resolution region as used in the run without star formation and feedback.

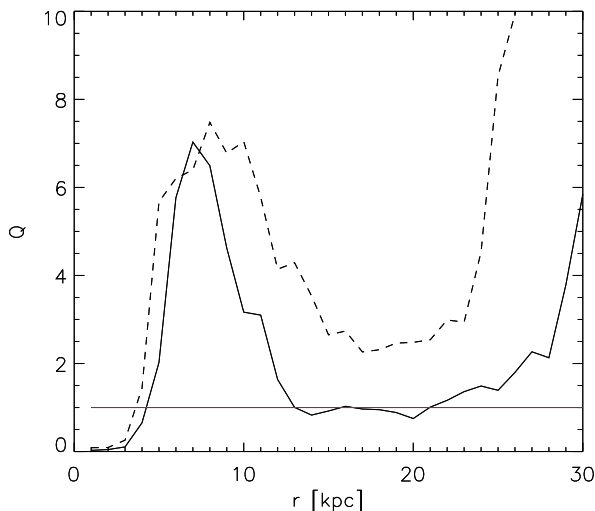


Figure 2. Disk stability is measured with the Toomre Q parameter in our 32^3 sphere. The solid horizontal line shows the stability criterion $Q > 1$. The solid curve is for the standard model, the dashed curve for the model with 5×10^4 K minimum gas temperature.

following four assumptions: (1) the disk mass is a fixed fraction of the halo mass ($m_d = M_{\text{disk}}/M_{\text{halo}}$), (2) the disk angular momentum is a fixed fraction of the halo angular momentum ($j_d = J_{\text{disk}}/J_{\text{halo}}$), (3) the disk is thin, centrifugally supported and has an exponential surface density profile, (4) only dynamically stable systems can correspond to real galaxies. The disk properties are then completely determined by the rotational velocity of the halo at r_{200} (the radius where $\rho(r) = 200\rho_c$), V_{200} , the concentration c of the halo, the spin parameter λ , m_d and j_d , and are calculated iteratively taking into account the influence of the forming disk on the halo density profile and rotation curve. This is a gravitational influence as well as a contraction of the inner regions of the halo.

As input parameters we use the results from our simulations, the disk mass M_d and disk angular momentum J_{disk} from

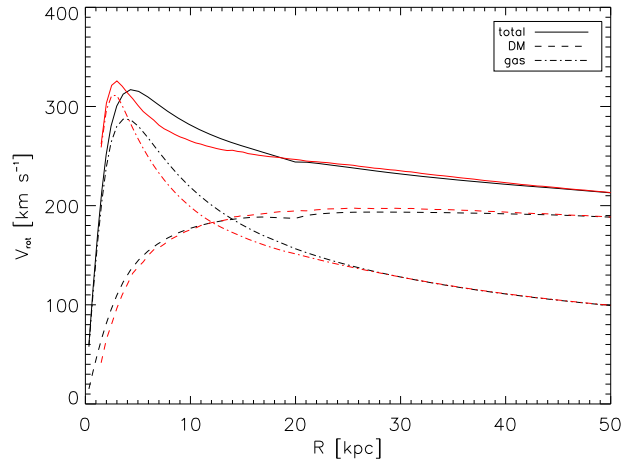


Figure 3. Comparison of the rotation curves from the simulation (red) and predicted by the MMW model (black).

the run with radiative cooling, and the dark matter halo parameters (halo mass M_{200} , halo angular momentum J_{200} , halo concentration c , spin parameter λ) from the pure dark matter run (note the use of R_{200} instead of R_{vir} here, to define the halo in agreement with MMW). For our purposes we mainly look at the predicted rotation curves for the disk and dark matter halo, which we then compare to the rotation curves obtained in our simulations. Table 2 gives the MMW parameters for the different runs. We applied two major modifications to the original MMW model. MMW assume an NFW halo with a density profile given by

$$\rho(r) = \rho_c \frac{\delta_c}{(r/r_s)(1+r/r_s)^2}, \quad (10)$$

where δ_c is a characteristic density and r_s is a scale length. Since our initial conditions are only semi-cosmological and we are missing the surrounding large scale structure, we are also missing some late infall of material into our halo which would happen in a fully cosmological box. This results in density profiles which deviate from a typical NFW profile at

large radii. Therefore, instead of using a halo mass profile based on the NFW profile as done by MMW, we use the calculated mass profile of the dark matter halo as an input for the model.

A second problem we encountered was a systematic over-prediction of the inner part of the dark matter rotation curve by the MMW model. As already mentioned above, the mass profile of the halo is influenced by the formation of the disk. This effect is described by the adiabatic contraction model, based on work by Barnes & White (1984) and Blumenthal et al. (1986). In this model, particles are assumed to move on circular orbits and angular momentum is strictly conserved. For circular orbits, the force is $F/m = v^2/r$ and the angular momentum is $j/m = vr$. Combining them and including angular momentum conservation leads to the general result for a particle starting at radius r_i and ending at radius r_f

$$F_f(r_f)r_f^3 = F(r_i)r_i^3. \quad (11)$$

With the Newtonian force law $F/m = \frac{GM(r)}{r^2}$, this leads to $M_f(r_f)r_f = M_i(r_i)r_i$, where $M(r)$ is the enclosed mass at radius r . This is the form used by MMW. However, in order to reduce the occurrence of two-body direct interactions in the simulations, the forces are softened and may be described rather with a Plummer force law

$$F_{Plummer} = \frac{-GMmr}{(r^2 + \epsilon^2)^{3/2}}. \quad (12)$$

We therefore modify the MMW model by using the force profile instead of the mass profile to calculate the adiabatic contraction (Gottbrath 2001). The force profile is given by

$$F(r) = \int F(S, r) dS \quad (13)$$

where $F(S, r)$ is the Plummer force profile of a spherical shell with radius S which in turn is given by

$$\frac{dF}{dS} = -\frac{GmM}{2r^2S} \left(\frac{\epsilon^2 + S(r+S)}{\sqrt{\epsilon^2 + (r+S)^2}} - \frac{\epsilon^2 + S(S-r)}{\sqrt{\epsilon^2 + (r-S)^2}} \right). \quad (14)$$

With this modified approach we achieve good agreement between the rotation curves predicted from the model and produced in the simulation, as can be seen in Figure 3. The only region being different is the inner 15 kpc of the disk rotation curve, which is much more peaked in the simulations. This is due to the high concentration of matter in the center as a result of the angular momentum problem, and to a lack of resolution in the center. The central clump behaves like a bar, sweeping up gas directly surrounding it and resulting in an underdense shell between the central clump and the thin disk. This is also visible in the bottom right plot of the disk in Figure 1. Therefore, the rotation curve is too peaked in the very center, and too low between radii of 5 and 18 kpc.

3.1.3 The angular momentum analysis

We analyze the loss of angular momentum by calculating in all snapshots the specific angular momentum of cold gas particles within a radius of 250 kpc (which is the virial radius at $z=0$). Since most cold gas particles end up in the disk, this basically traces the angular momentum evolution of disk

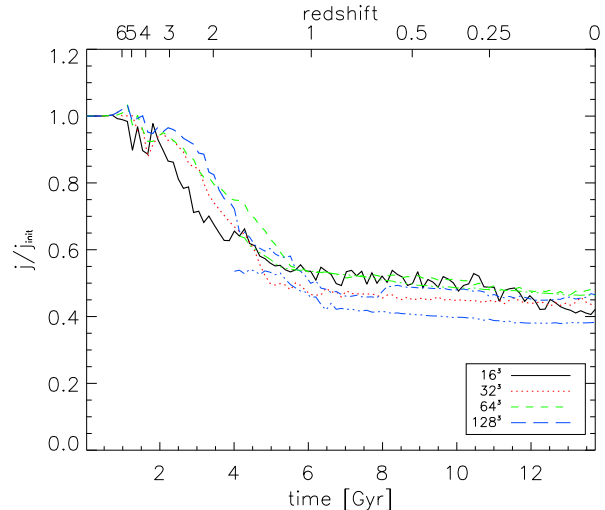


Figure 4. The evolution of the specific angular momentum over time for the cold gas within the virial radius. The different colored lines show the 4 different resolutions of the semi-cosmological halos. The dash-dotted and dash-double-dotted parts of the blue line indicate the evolution for the highest resolution case, when gas was converted to stars, calculated in two different ways. As a comparison, this was also done for the 64^3 resolution, shown in the green dash-double-dotted line.

particles. The result is shown in Figure 4. The highest resolution run (128^3 particles in the underlying box, blue line) poses a computational challenge. Without star formation, it is computationally infeasible to advance the simulation beyond $z \sim 1.7$. We overcome this by replacing all gas particles at this point with collisionless “star” particles. In this way, no further cooling is possible, but the disk is already largely in place at this point. Reducing the computation to only gravitational forces enables us to extend the run until $z=0$. For the angular momentum calculation until $z=1.7$, we use the cold gas within the virial radius, as in the other resolutions. After that we follow two different methods. First we tested to use all star particles within the virial radius (thin, dash-dotted blue line). However, in a comparison of the same procedure for the 64^3 resolution, we find much better agreement with the original gas run when following only the stars making up the galaxy at $z=0$ (all star particles in a radius of 50 kpc). This is shown in the thin green dash-dotted line. Applying the same procedure to the 128^3 resolution results in the lower, blue dash-triple-dotted line. The discontinuity to the gas run at $z=1.7$ is due to the switch in calculation methods. The resulting angular momentum evolution of the two calculation methods are not very different. The result of the real gas disk is expected to be in between the two. In both cases, there is good agreement with the evolution in the lower resolution runs, strongly indicating a gravitational effect as the reason for the angular momentum loss and ruling out artefacts from the hydrodynamics or SPH implementation in the code. The behavior in all four resolutions is quite similar. For the highest resolution the loss is slightly stronger, indicating that resolution makes the problem more severe instead of improving it. We first calculate

resolution	R_{200} [kpc]	V_{200} [km s ⁻¹]	M_{200} [M_{\odot}]	j_{200} [kpc km s ⁻¹]	j_{disk} [M_{\odot}]	j_{disk} [kpc km s ⁻¹]	m_d	j_d
16 ³	189	138.24	8.36×10^{11}	2233.25	1.09×10^{11}	1017.6	0.13	0.059
32 ³	191	139.42	8.59×10^{11}	2100.72	1.15×10^{11}	1092.4	0.134	0.07
64 ³	192	139.47	8.64×10^{11}	2230.24	1.2×10^{11}	1234.8	0.139	0.077

Table 2. Parameters for the MMW model.

the ratio of the final over the initial specific angular momentum of the disk particles for our four resolutions. Over our entire resolution range we find the same net loss of angular momentum of about 55% and no trend with resolution is observed. This indicates that a simple increase in resolution does not help to alleviate the angular momentum problem within the framework of the basic hierarchical model of galaxy formation.

We now investigate, when and how the angular momentum is lost. In combination with Figure 1, Figure 4 clearly illustrates that the bulk of angular momentum is lost during the phase of evolution dominated by the infall and merging of smaller clumps. At $z=1$, the angular momentum ratio is $j_{z=1}/j_{\text{init}} \sim 0.55$. Once the disk is established at $z \sim 1$, there is still some loss, but this happens gradually with $j_{\text{final}}/j_{z=1} \sim 0.88$. This further illustrates that improved resolution does not strongly influence this process, since the loss not only follows the same pattern in all resolutions, it also would otherwise continue stronger even after the formation of the disk. We can further strengthen our conclusion by following Weil, Eke & Efstathiou (1998) and evolving the gas component adiabatically until $z=1$. The lack of radiative cooling prevents the formation and therefore merging of small clumps in the gas. The disk forms quickly after the cooling is turned on at $z=1$. Figure 5 shows the resulting difference for the gas in the 32³ run. There is still a loss of angular momentum, but it is smaller than before, with a final ratio for the disk of $j_{\text{final}}/j_{\text{init}}=68.3\%$ and $j_{z=1}/j_{\text{init}}=95.1\%$ at $z=1$.

3.2 Cosmological initial conditions

We now turn our attention to the angular momentum problem in a fully cosmological run to verify our conclusions. For this we use the medium resolution cosmological halo, with 1024³ particles effective resolution in the high resolution region. Characteristic parameters of the halo and disk can be found in Table 1.

The disk in this case is as centrally concentrated as in the semi-cosmological case with 78% of the disk gas within the central 5 kpc. The build-up of the gas disk is shown in Figure 6. The top and middle panels have a side length of $1 h^{-1}$ Mpc in comoving coordinates and nicely show the hierarchical growth from small clumps to larger objects. In the time between the two middle panels ($z \sim 1.5$ and $z \sim 0.75$) a last larger merger of two gas clumps occurs. After that, the disk grows only via accretion. The bottom panel zooms into the disk before and after that merger. It is interesting to now compare (see Figure 7) the mass growth history of the disk (solid line) and the evolution of the specific angular

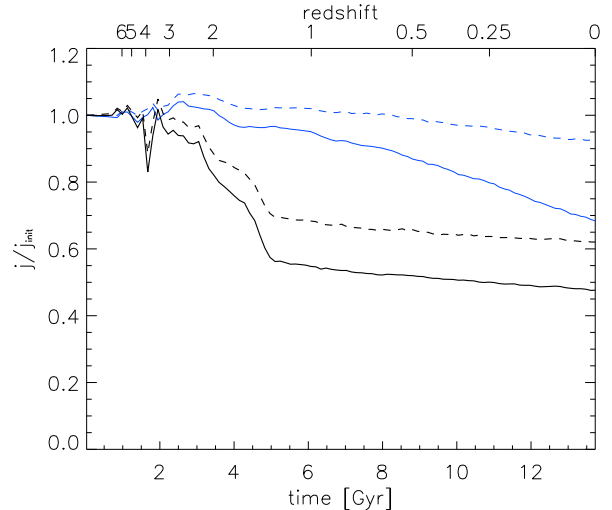


Figure 5. Comparing the angular momentum evolution for the 32³ halo in the standard case (with radiative cooling switched on all the time, black thick curves) with the run with adiabatic evolution until $z=1$ and cooling after $z=1$ (blue thin curves). The solid lines are for disk gas, the dashed lines for all gas within the virial radius at $z=0$.

momentum of the disk particles (dashed line). The arrows indicate the points in time at which the snapshots in Figure 6 are shown. The early growth of angular momentum accompanying the first collapse of the halo follows well the expectations from tidal torque theory (Jct). The maximum angular momentum acquired by the gas agrees well with the angular momentum of the dark matter halo. However, it can clearly be seen, that in particular the merger of two large gas clumps at $z \approx 1.5$, which increases the mass of the disk by about 25%, is accompanied by a large loss in angular momentum (about 50%). The ratio of final to maximum specific angular momentum is 0.37. This is a little less than what we found in the semi-cosmological case, as expected, thus confirming and even strengthening our conclusions of the previous section.

4 THE INFLUENCE OF STAR FORMATION AND STELLAR FEEDBACK ON THE ANGULAR MOMENTUM PROBLEM

In Figure 8, we show the gas and stellar component of the resulting galaxy in our simulations including star formation

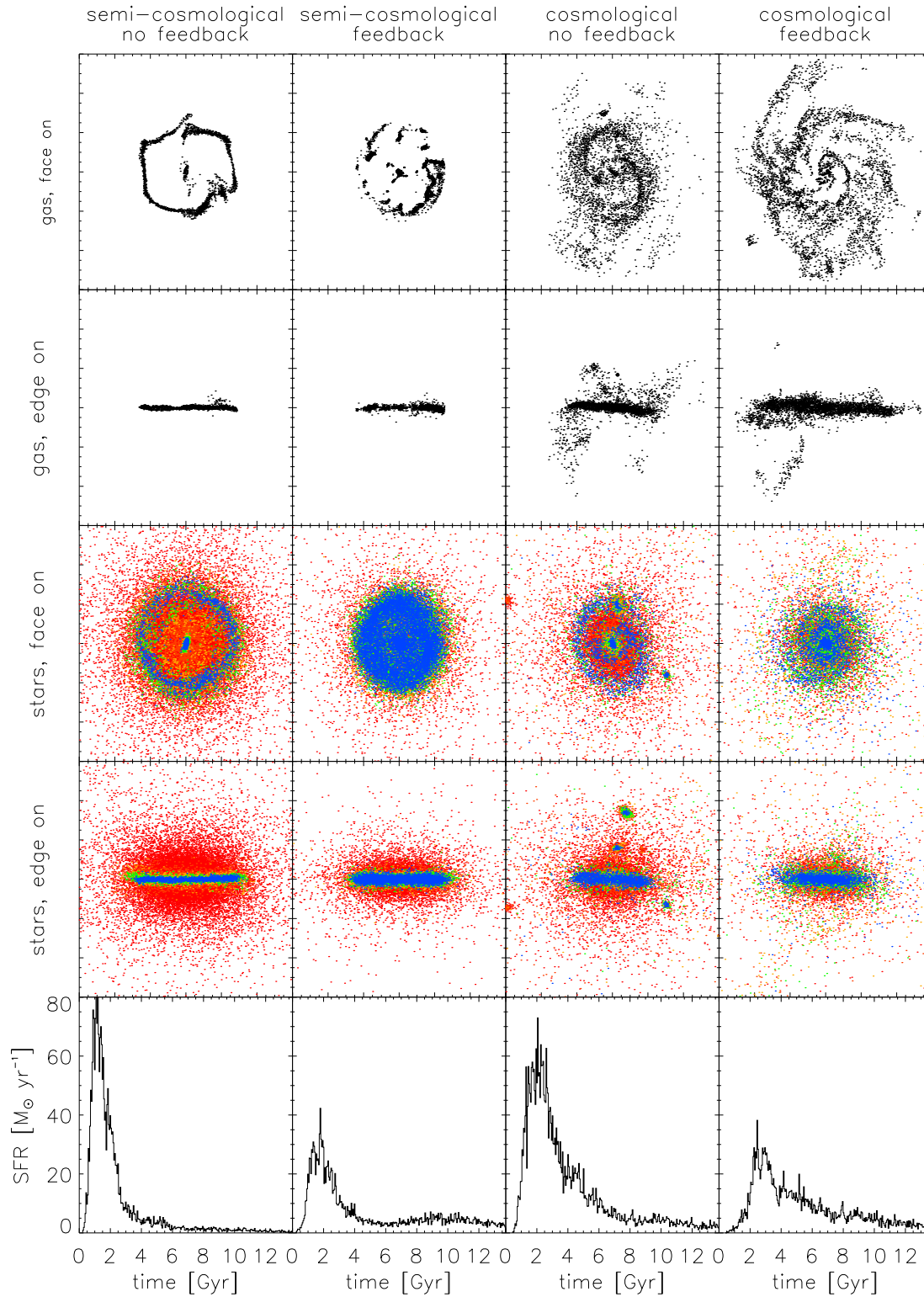


Figure 8. Results at $z=0$ of the runs with star formation. In the first and third columns we show runs without feedback, and runs with feedback are displayed in the second and fourth column. The left two columns are semi-cosmological results, the right two columns are fully cosmological runs. The face on and edge on plots have a side length of 80 kpc. The top two rows show the cold gaseous disk, rows 3 and 4 the stellar component. The star particles are color-coded by age (red: older than 10 Gyr, blue: younger than 4 Gyr). The bottom row shows the star formation history.

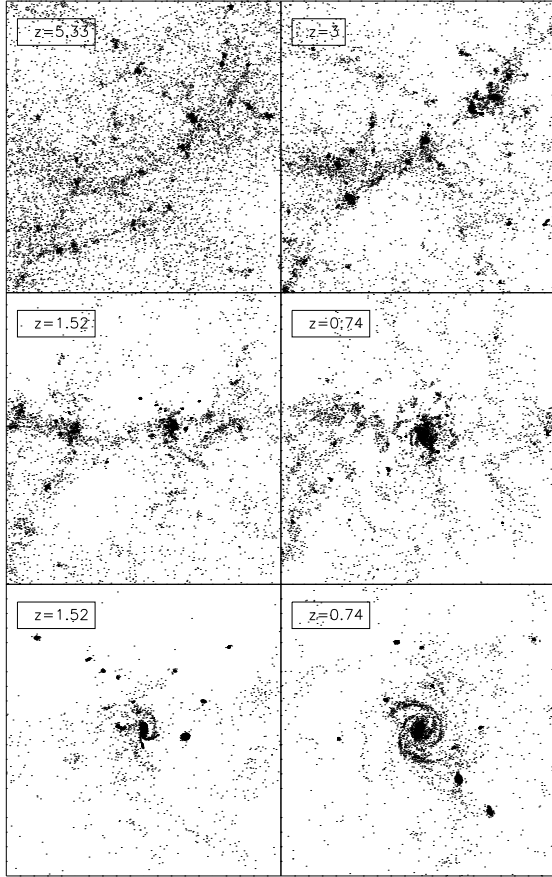


Figure 6. Snapshots illustrating the assembly of the gas disk in the fully cosmological runs. The top four plots have a side length of $1000 \text{ comoving kpc h}^{-1}$ to show the larger environment, the bottom two plots zoom in to show more clearly the disk itself and has a side length of 200 kpc h^{-1} in physical coordinates.

(columns 1 and 3 for the semi- and the cosmological environments, respectively) and including star formation and feedback (columns 2 and 4 for the semi- and the cosmological environments, respectively). The first feature to notice is the ring-like structure of the gas disk in the semi-cosmological runs (top row, columns 1 and 2). The reason for this is the efficient transformation of gas into stars moving inside-out, and the missing late infall of gas to replenish the disk. The disk here is also much more defined than in the fully cosmological case, again due to the missing influence of late incoming clumps. In all cases, the young stars (younger than 4 Gyr, colored in blue) and the cold gas ($T \leq 3 \times 10^4 \text{ K}$) form a fairly thin disk. In both the semi-cosmological and the fully cosmological run without feedback (column 1 and 3) stars are formed very efficiently at early times, resulting in a dominant spheroidal component. This can also be seen in the strong peak in the star formation history at a $t \approx 2 \text{ Gyr}$ (bottom row). When feedback is included (column 2 and 4), star formation is quenched efficiently and a more prominent disk of young stars is formed while the large spheroidal component made up of old stars (colored red) is reduced. It is also

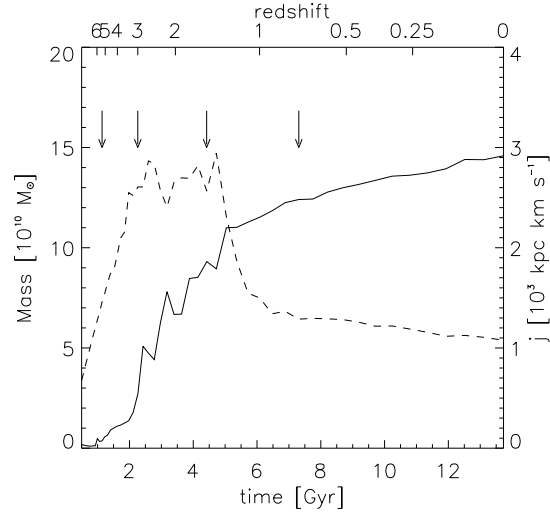


Figure 7. Growth of the disk (solid line) and evolution of angular momentum (dashed line) for the fully cosmological run. The big loss in angular momentum starting at $z=1.5$ clearly coincides with a large mass increase. The arrows indicate the time of the snapshots shown in Figure 6.

noticeable, that the gas disk is much more extended than the young stellar component in the cosmological runs. This is in agreement with observations (for example Boomsma et al. 2008).

4.1 The origin of the stellar components

Why do we find such a large spheroidal component in the runs without feedback, even though the gas disk in the runs without star formation is very thin? The answer can be found in the location and the time where the stars are formed. In our fully cosmological run, star formation starts at $z \sim 9$, and it peaks at $z \sim 3$. This is the time when the progenitor of the $z=0$ disk is just starting to be assembled, so the majority of the stars are actually forming in larger mass clumps which fall in until $z \sim 1.2$. After that, mass grows more slowly through accretion and the infall of smaller clumps. Stars are continuously formed in the disk progenitor, but at a very low rate of about $2 \text{ M}_\odot \text{ yr}^{-1}$. The stars entering the halo in clumps are not able to settle into a disk and therefore will form a spheroid. Only the stars formed within the disk progenitor will be rotationally supported and can form a stellar disk. This can be seen in Figure 9, which shows the distribution of stars at $z=0$, divided according to their formation environment into “clump stars” (stars formed outside of the disk progenitors and assembled into the galaxy via merging) and “disk stars” (stars formed in the progenitor of the $z=0$ disk). “Disk stars” form a reasonably thin distribution tracing the gas disk, “clump stars” make up the large spheroid. One important diagnostic of the nature of the stars is the ratio of rotational velocity to velocity dispersion. Both parameters are plotted in Figure 10 for all stars (black line), “clump stars” (red line) and “disk stars” (blue line). For “disk stars”, this ratio is much higher, confirming their rotational support compared to dissipational

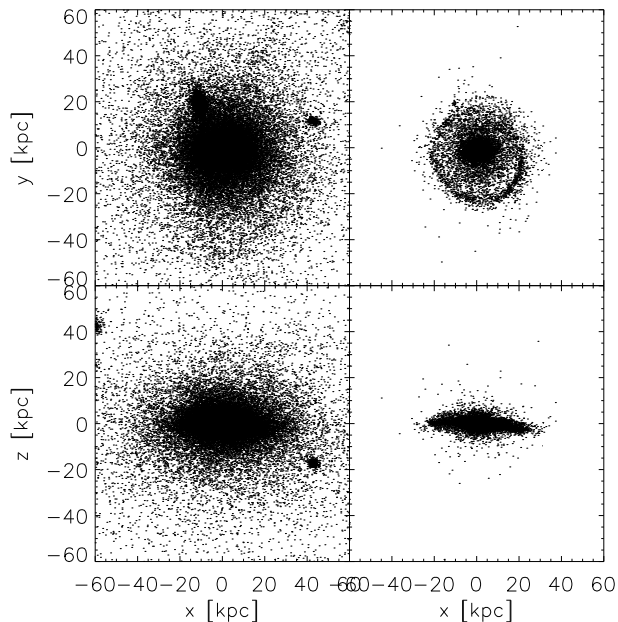


Figure 9. Face-on and edge-on projection of the stars at redshift 0. The left column shows the stars which were formed in clumps and then accreted. The right column shows the stars which were formed in the disk progenitor.

support for "clump stars". Of all stars in the galaxy at $z=0$, 30% are "disk stars" and 70% are "clump stars". We performed a test where star formation was only turned on at $z=1$, with the thin gas disk being more or less in place and further mass infall mostly through smooth accretion. The stars in this case indeed form a very prominent stellar disk, but no large spheroidal component.

In the feedback runs, star formation also begins early in individual clumps. The feedback however heats the gas and pushes it out of these structures, quenching the star formation in the clumps and enabling the gas to be accreted smoothly later directly into the disk where it then can form disk stars. This is evident from the reduced early star formation peak in the feedback runs as shown in Figure 8. Consequently, in the final galaxy we have only 35% of all stars formed in clumps (and therefore a much less prominent spheroidal component as visible in Figure 8 right column) and 64% formed in the disk progenitor.

4.2 The angular momentum problem

Since now gas particles are converted into stars, we compute the angular momentum for the combination of cold gas and stars. The result for the semi-cosmological runs is shown in Figure 11(a). The loss is smaller when including star formation (dashed line), but still substantial. In the case with feedback (dotted-dashed line), later accretion of gas with high angular momentum keeps the angular momentum of the disk high and the final galaxy has almost 90% of the initial angular momentum. Gas is available for late accretion due to the decreased early star formation. The results for the cosmological runs are shown in Figure 11(b). We are track-

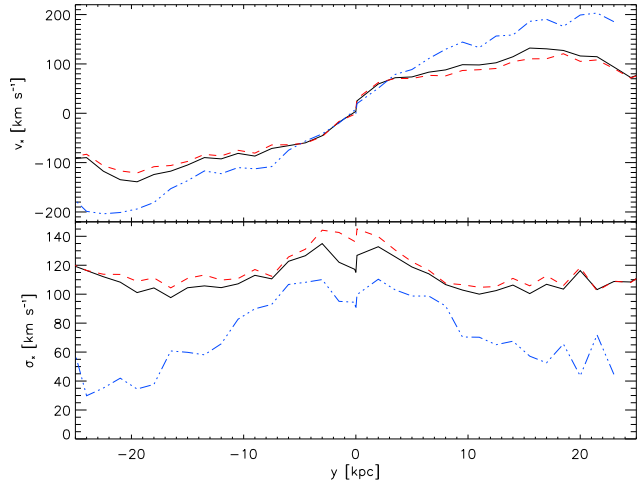


Figure 10. Rotational velocity (top) and velocity dispersion (bottom) of all stars (black, solid line), "clump stars" (red, dashed line) and "disk stars" (blue, dash-triple-dotted line).

ing the cold gas and stars of the final galaxy at $z=0$ over time. In all three cases we see a drop in angular momentum at $z\sim 1.2$, but it is less pronounced in runs with star formation and even smaller in those with feedback. However, in simulations with star formation there is some loss of angular momentum after $z=1$, which is not as significant when only cooling is employed. This is probably due to the increased late accretion of gas and related hydrodynamical torques. Compared to the maximum angular momentum, an even slightly higher percentage is lost in the case with star formation, and still about 50% with feedback. Most of this loss occurs after $z=1$. The feedback has reduced the loss owing to dynamical friction but increased the later loss due to hydrodynamical torques. While a loss of 50% still seems large, this is consistent with expectations comparing dark matter halos and observed disks (Navarro & Steinmetz 2000). For the feedback case, we plot the results of runs with three different resolutions (effective resolutions of 512^3 , 1024^3 and 2048^3), which behave similarly indicating that resolution does not affect this process much. We conclude that feedback in both the semi-cosmological and the cosmological simulations clearly helps to alleviate the angular momentum problem which is mainly due to the reduction of the early star formation and the resulting smaller spheroidal component.

5 SUMMARY AND CONCLUSIONS

In this paper we have studied the causes of the angular momentum problem with special emphasis on the influence of numerical resolution and the impact of star formation and feedback. We performed a systematic study leading us from a controlled, isolated, "semi-cosmological" experiment to fully cosmological simulations. We also investigated simulations with different physical processes, once only taking into account radiative cooling, then including simple star formation and finally also including supernova feedback. The advantage of the semi-cosmological environment is to combine at moderate computational costs an

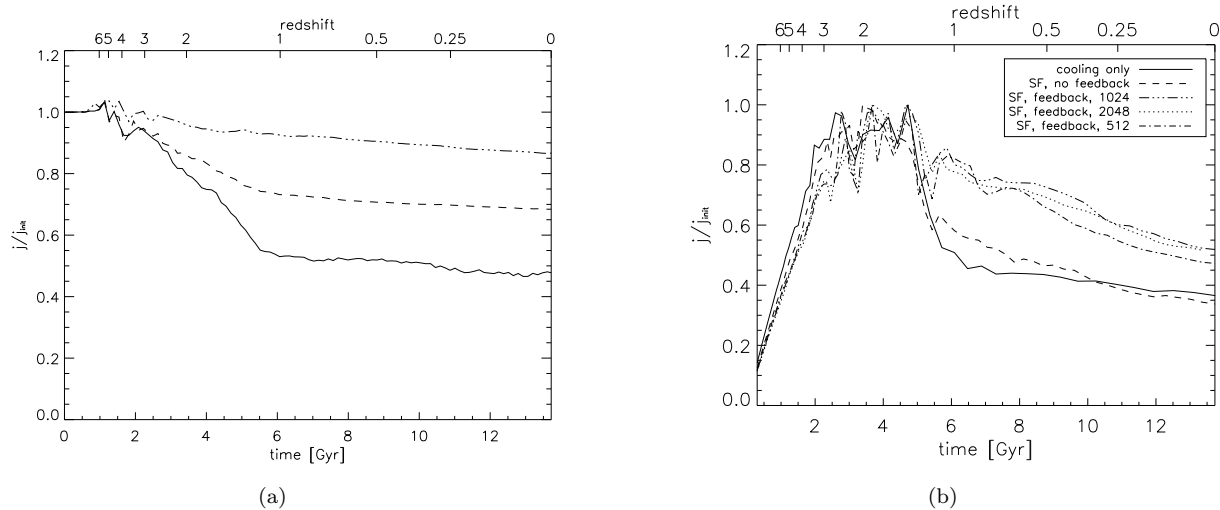


Figure 11. These plots compare the specific angular momentum evolution in the runs without star formation (solid line), with star formation but without feedback (dashed line) and with star formation and feedback (dashed-dotted line). Panel (a) shows the semi-cosmological, panel (b) the fully cosmological runs. The three different lines for feedback in Panel (b) show runs with three different resolutions.

isolated, well controlled halo with the small scale hierarchical buildup which is characteristic for a Λ CDM universe. By performing first simulations without star formation, it is possible to assess the importance of resolution in the hierarchical framework for structure formation, especially with respect to the angular momentum problem. Our results clearly show that an increase in resolution in this case does not help against the angular momentum loss. The loss of angular momentum for the disk gas is of the same order while the resolution changes by orders of magnitude. We are also able to tie the angular momentum loss to the phase of collapse into small cold gas clumps which merge and form the main object. The main loss mechanism is dynamical friction of the clumps and larger mergers, as shown by Navarro & Benz (1991), Navarro & White (1994), Navarro & Steinmetz (1997), d’Onghia et al. (2006) and Zavala et al. (2008). The efficiency of dynamical friction is dominated by the largest clumps. These clumps can be tracked even in low resolution simulations (Gao et al. 2004, and references therein). This explains why, contrary to for example Kaufmann et al. (2007), we find no significant resolution dependence even though our resolution range is comparable. Kaufmann et al. (2007) studied the formation of a gas disk starting in an equilibrium halo without taking the halo formation history into account, so their angular momentum loss is mainly due to hydrodynamical and gravitational torques during gas infall. This is a resolution-dependent process. We also see this effect, as can be seen in the run with cooling switched on only after $z=1$ (Figure 5) and in the cosmological runs with star formation and feedback. However, the effect is much smaller than the loss during the merger period. We therefore argue that, in order to prevent the angular momentum loss in cosmological simulations, mainly the early formation of gas and star clumps must be prevented. The loss owing to limited numerical resolution appears to be only of second order. In line with this argument, we observe a comparable loss in our fully cos-

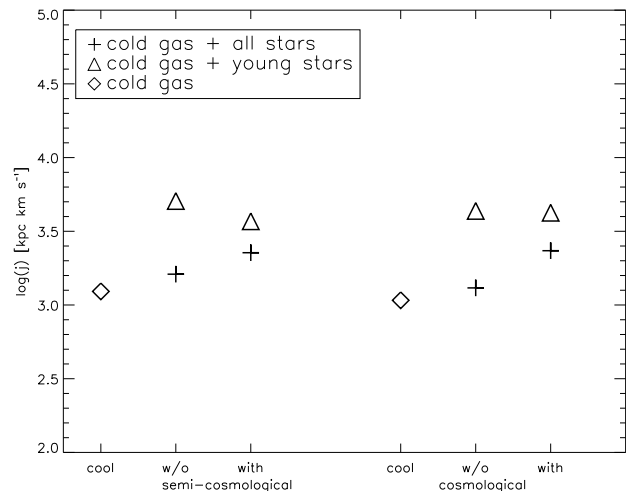


Figure 12. For the semi-cosmological and cosmological run, we compare the final angular momentum of the disk in the cooling run (“cool”), with star formation but without feedback (“w/o”) and with feedback (“with”). The disk angular momentum is computed once including the cold gas disk and all stars in the galaxy (crosses), and also including the cold gas and the young stars only (triangles).

mological simulation. It can be clearly linked again to the merging of two large gas clumps. Unfortunately it is computationally not feasible to run this at higher resolution without star formation. However, even if resolution would have some influence in cosmological simulations (contrary to the semi-cosmological case), this would only make the problem worse by increasing the number of resolved gas clumps. We are confident that this would not lead us to a different conclusion.

The most plausible mechanism to prevent clump for-

mation is star formation and related supernova feedback because it heats the gas. Another possible source of heating would be the cosmic UV background. Some low resolution tests we performed including this effect did not show any positive impact. Indeed, Navarro & Steinmetz (1997) showed that a UV background may even have an adverse effect as it suppresses the infall of gas which is accreted late in the formation history and thus acquired high angular momentum. Here we show the changes in the angular momentum evolution when star formation and supernova feedback is included. As expected, star formation alone does not result in an improvement, since the same clumps are spiraling in. They simply consist of highly condensed stars instead of highly condensed gas. Star formation peaks high early on, and especially in the semi-cosmological setup, where late gas infall is missing, most gas is used up at $z=0$. Feedback helps to prevent this by keeping the gas too hot to form stars and therefore allowing it to settle into the disk later on as high angular momentum gas. We studied the origin of the stars in the final galaxy and found that without feedback 70% of all stars in the final galaxy enter in clumps. With feedback this is reduced to 35%. This can also be seen in the angular momentum of the final galaxy. Clump stars form a slowly rotating spheroidal component and disk stars form a rotationally supported, high angular momentum disk. The final angular momentum of the gas and all stars combined is therefore much higher in our runs with feedback (and a smaller spheroid) than in the ones without feedback (and a large spheroid). This is further illustrated when looking at the combined angular momentum of the rotationally supported component of the galaxy, consisting of the cold gas and the young stars only (Figure 12). This is roughly equal in the runs with and without feedback (triangles), while for the total galactic angular momentum including all stars a clear increase can be seen from the run including only radiative cooling over the run with star formation to the run with star formation and feedback. This increase is due to the decrease of the central gas clump and then of the stellar spheroid.

We conclude that an efficient suppression of the formation of dense clumps at early times is the main factor in reducing the angular momentum loss. Star formation alone cannot provide this effect since these dense gas clumps also fulfill the conditions for star formation resulting in a high early star formation peak and the formation of a large bulge. Only feedback can reduce this effect efficiently. Resolution overall plays a secondary role. In our simulations with star formation and feedback, the angular momentum loss is about 50% which is in agreement with expectations from comparisons between dark matter halos and observed disk galaxies (Navarro & Steinmetz 2000). This loss mainly happens at late times due to hydrodynamical torques. In our simulations with three levels of resolution in the cosmological halo, resolution does not influence this effect either. While feedback has such a critical role in the formation of more realistic disks in simulations, it is still not well understood. In Piontek & Steinmetz (2009b) we therefore present a detailed study of stellar feedback in disk formation simulations.

ACKNOWLEDGEMENTS

We thank Stefan Gottlöber and Gustavo Yepes for providing initial conditions and Volker Springel for providing a version of GADGET2 which included radiative cooling. This work was funded through a grant by the German Research Foundation (DFG) under STE 710/4 as part of the Priority Programme SPP1177 "Witnesses of Cosmic History: Formation and evolution of black holes, galaxies and their environment".

REFERENCES

- Barnes, J., White, S.D.M., 1984, MNRAS, 211, 753
 Barnes, J., Efstathiou, G., 1987, ApJ, 319, 575
 Blumenthal, G.R., Faber, S.M., Flores, R., Primack, J.R., 1986, ApJ, 301, 27
 Boomsma, R., Oosterloo, T.A., Fraternali, F., van der Hulst, J.M., Sancisi, R., 2008, A&A, 490, 555
 Bullock, J.S., Dekel, A., Kolatt, T.S., Kravtsov, A.V., Klypin, A.A., Porciani, C., Primack, J.R., 2001, ApJ, 555, 240
 Doroshkevich, A.G., 1970, Astrofizika, 6, 581
 D'Onghia, E., Burkert, A., Murante, G., Khochfar, S., 2006, MNRAS, 372, 1525
 Duerr, R., Imhoff, C.L., Lada, C.J., 1982, ApJ, 261, 135
 Fall, S.M., Efstathiou, G., 1980, MNRAS, 193, 189
 Gao, L., White, S.D.M., Jenkins, A., Stoehr, F., Springel, V., 2004, MNRAS, 355, 819
 Gerritsen, J.P.E., 1997, PhD thesis, Kapteyn Astron.Inst., The Netherlands
 Gingold, R.A., Monaghan, J.J., 1977, MNRAS, 181, 375
 Götz, M., Sommer-Larsen, J., 2003, Ap&SS, 284, 341
 Gottbrath, C., 2001, Master's thesis, University of Arizona, USA
 Governato, F., Mayer, L., Wadsley, J., Gardner, J.P., Willman, B., Hayashi, E., Quinn, T., Stadel, J., Lake, G., 2004, ApJ, 607, 688
 Hoyle, F., 1949, in *Problems of Cosmical Aerodynamics* (Dayton, Ohio: Central Air Documents Office), p. 195
 Katz, N., 1991, ApJ, 368, 325
 Katz, N., 1992, ApJ, 391, 502
 Katz, N., Weinberg, D.H., Hernquist, L., 1996, ApJS, 105, 19
 Kaufmann, T., Mayer, L., Wadsley, J., Stadel, J., Moore, B., 2007, MNRAS, 375, 53
 Kautsch, S.J., Grebel, E.K., Barazza, F.D., Gallagher, J.S., III, 2006, A&A, 445, 765
 Lokas, E.L., Hoffman, Y., 2001, arXiv:astro-ph/0112031
 Lucy, L.B., 1977, ApJ, 82, 1013
 Mayer, L., 2005, Proceedings of Science, volume of the Conference "Baryons in Dark Matter halos", edited by P. Salucci, Novigrad, Croatia
 Miller, G.E., Scalo, J.M., 1979, ApJS, 41, 51
 Mo, H.J., Mao, S., White, S.D.M., 1998, MNRAS, 295, 319
 Navarro, J.F., Benz, W., 1991, ApJ, 380, 320
 Navarro, J.F., White, S.D.M., 1994, MNRAS, 267, 401
 Navarro, J.F., Frenk, C.S., White, S.D.M., 1997, ApJ, 490, 493
 Navarro, J.F., Steinmetz, M., 1997, ApJ, 478, 13
 Navarro, J.F., Steinmetz, M., 2000, ApJ, 538, 447

- Okamoto, T., Eke, V.r., Frenck, C.S., Jenkins, A., 2005, MNRAS, 363, 1299
- Peebles, P.J.E., 1969, ApJ, 155, 393
- Piontek, F., Steinmetz, M., 2009, submitted to MNRAS
- Power, C., Navarro, J.F., Jenkins, A., Frenk, C.S., White, S.D.M., Springel, V., Stadel, J., Quinn, T., 2003, MNRAS, 338, 14
- Robertson, B., Yoshida, N., Springel, V., Hernquist, L., 2004, ApJ, 606, 32
- Schmidt, M., 1995, ApJ, 129, 243
- Sommer-Larsen, J., Dolgov, A., 2001, ApJ, 551, 608
- Spergel, D.N. et al., 2007, ApJS, 170, 377
- Springel, V., 2005, MNRAS, 364, 1105
- Steinmetz, M., Bartelmann, M., 1995, MNRAS, 272, 570
- Steinmetz, M., Müller, E., 1995, MNRAS, 276, 549
- Steinmetz, M., Navarro, J.F., 1999, ApJ, 513, 555
- Steinmetz, M., White, S.D.M., 1997, MNRAS, 288, 545
- Strömberg, G., 1934, ApJ, 79, 460
- Thacker, R.J., Couchman, H.M.P., 2000, ApJ, 545, 728
- Toomre, A., 1964, ApJ, 139, 1217
- Toomre, A., Toomre, J., 1972, ApJ, 178, 623
- Viel, M., Becker, G.D., Bolton, J.S., Haehnelt, M.G., Rauch, M., Sargent, W.L.W., 2008, PhRvL, 100, 041304
- Weil, M.L., Eke, V.R., Efstathiou, G., 1998, MNRAS, 300, 773
- White, S.D.M., Rees, M.J., 1978, MNRAS, 183, 341
- White, S.D.M., 1984, ApJ, 286, 38
- Zavala, J., Okamoto, T., Frenk, C.S., 2008, MNRAS, 387, 364